Journal of Naval Architecture and Marine Engineering
January, 2026
https://dx.doi.org/10.3329/jname.v23i1.81886 https://www.banglajol.info

OPTIMIZATION OF ELECTRIC PROPULSION SYSTEMS FOR FERRY VESSELS: A CASE STUDY IN RIVERINE OPERATIONS

Budhi Santoso[1]*, Romadhoni[1], Johny Custer[2], Zulfaidah Ariyany[3]
[1]Department of Naval Architecture, Polytechnic of Bengkalis, 28711, Indonesia
[2]Department of Electrical, Polytecnic of Bengkalis, Bengkalis, 28711, Indonesia
[3]Department of Industrial Technology, Vocational College, Universitas Diponegoro, Semarang, 50275, Indonesia

Abstract:

This study aims to design, optimize, and validate an all-electric propulsion system for a 25 m × 7 m aluminum catamaran ferry operating on a 25 km urban river route, focusing on power requirement prediction, battery sizing, energy-management strategies, and shore-charging integration. A slender-body resistance model, validated by cubic speed–power scaling, predicts calm-water resistance rising from 18.5 kN at 12 knot to 43.8 kN at the contractual speed 19 knot. Accounting for hull and drivetrain efficiencies yields a continuous shaft power requirement of 707 kW. Two 360° Hydromaster D-series azimuth thrusters driven by 375 kW permanent-magnet motors are selected, providing 6 % continuous head-room and full redundancy while avoiding the mass penalty of a single 1 MW unit. Daily energy demand is quantified via a mode-based load matrix distinguishing propulsion, hotel, and intermittent peaks. Twelve round trips within a 17 h duty window consume 16.1 MWh for propulsion and 0.09 MWh for auxiliaries (16.2 MWh total). Limiting depth-of-discharge to 80% and reserving 20% state-of-charge for emergencies yields a 20.3 MWh lithium-iron-phosphate battery bank (204×100 kWh modules; 127 t, 68 m³) fitted amidships. Opportunity charging during each 25 min turnaround with a 6 MW liquid-cooled DC connector restores 1.7 MWh per call, maintaining the pack between 40% and 80% SOC and eliminating the need for 20–48 MW fast-charge infrastructure. This paper applies a Genetic Algorithm (GA) to optimize the decision vector P_{thr}, C_{bat}, P_{chg}, yielding a 12 % reduction in daily energy consumption compared to the baseline design. Convergence behaviour, optimal parameter values, and trade-offs between energy and capital cost are presented. Load-levelling strategies—radar standby, demand-controlled ventilation, and regenerative braking—trim hotel consumption by up to 15 % and reduce peak inverter currents. Sensitivity analysis shows that lowering service speed to 17 knot cuts daily energy by 23%, highlighting the trade-off between timetable and shore-power investment. By integrating resistance prediction, thruster selection, battery sizing, and charging strategy into a single framework, this research demonstrates the technical and operational feasibility of zero-emission river ferries and provides a repeatable methodology for future deployments in similarly constrained waterways.

Keywords: Electric propulsion, ferry vessel, ship electrical load, power balance, renewable energy, propulsion energy

NOMENCLATURE

P	propulsion-power requirement, kW
F	total hydrodynamic resistance, N
V	ship speed in still water, m s^{-1}
L, B, D, T	principal hull dimensions (length, breadth, depth, draft), m
E	energy demand per duty cycle, kWh
P_{thr}	is the continuous power rating per azimuth thruster (kW)
C_{bat}	installed battery capacity, kWh

Greek symbols

η_H	hull (propeller–hull) efficiency
η_E	electrical drivetrain efficiency
λ	propulsion load factor (fraction of MCR)
ρ	water density, kg m^{-3}
ν	kinematic viscosity of water, m^2 s^{-1}
$Pchg$	is the peak shore-charging power (kW)
k	form-factor coefficient in resistance equation

1. Introduction

River transportation plays a vital role in enhancing connectivity and supporting economic activities worldwide. Ferry vessels are a critical component of this mode of transportation, serving as connectors between communities and facilitating commerce in various regions.(Cope et al., 2020). However, conventional ferries often rely on fossil fuels, contributing to greenhouse gas emissions and environmental degradation.(Trillos et al., 2021). The

1813-8535 (Print), 2070-8998 (Online) Received: May, 2025

need for sustainable and energy-efficient solutions has spurred interest in electric ferries equipped with advanced propulsion systems.(Al-Falahi et al., 2018a).
Electric propulsion systems have been recognized for their potential to reduce emissions, lower operational costs, and minimize noise pollution, making them ideal for operations in environmentally sensitive or densely populated areas.(Varga et al., 2020). Despite these advantages, the adoption of electric ferries presents unique challenges, particularly in riverine environments where varying currents, shallow water depths, and seasonal fluctuations in river conditions significantly impact vessel performance.(Gagatsi et al., 2016).

Previous studies have highlighted the energy efficiency and environmental benefits of electric propulsion systems in maritime applications(Ammar and Seddiek, 2021). However, there remains a research gap in understanding the performance of these systems under the specific conditions of riverine transportation. Factors such as power requirements, battery capacity, and charging infrastructure must be carefully analyzed to ensure the feasibility and reliability of electric ferry operations(Hasanvand et al., 2020).

This study aims to address this gap by designing and analyzing an electric propulsion system tailored for a ferry operating in riverine environments.(Al-Falahi et al., 2018b). The analysis focuses on the vessel's power requirements, battery system design, and overall energy efficiency.(Zhu et al., 2023). By providing insights into the operational feasibility and design optimization of electric ferries, this research contributes to the broader goal of achieving sustainable and environmentally friendly transportation solutions.(Oo et al., 2022).

2. Methodology

2.1 Power requirement determination

The first stage in designing an electric-propulsion system involves determining the vessel's power needs based on ship size, maximum speed, and other operational conditions, which is often done using empirical or analytical methods grounded in physical laws and prior data; for example, the basic power-requirement formula is as Equation (1), where P is the required propulsion power, F is the calm-water resistance, and υ is the vessel's speed, provides a simple yet fundamental starting point.

$$P=F\times\upsilon \tag{1}$$

Where F is the required force and v is the velocity.(Zhang et al., 2023).

In the context of maritime propulsion systems, power requirement analysis involves an assessment of various factors such as shipload, anticipated speed, and environmental conditions such as currents and wind. This analysis includes evaluating the ship's operational performance under various conditions and estimating the power needed for each of these conditions. This usually involves hydrodynamic models to understand how the ship interacts with water and using basic physics equations to estimate power needs.(Gupta et al., 2022).

2.1.1 Operational-mode matrix
As detailed in Table 1, the daily timetable is discretised into N operational modes mmm (sailing/departure, loading/unloading, and mooring/lay-up), with each mode characterised by a duration t_m (h), a continuous load $P_{c,m}$ (kW), and an intermittent peak $P_{i,m}$ (kW).

Table 1: The daily timetable is discretised into N modes m

Mode mm	Duration t_m (h)	Continuous load Pc,m (kW)	Intermittent peak Pi,m(kW)
Sailing/departure	t1t_1	PMCR	small
Loading/unloading	t2t_2	low	thruster peak
Mooring/lay-up	t3t_3	hotel only	capstan peak

2.2 Selection and design of electric motors

Electric motor design involves the selection of motor type e.g., AC or DC motor, synchronous or asynchronous motor, etc., size, and performance characteristics. This design also involves calculations such as efficiency, torque, and rotations per minute (RPM)(Bajrami and Palpacelli, 2023). An integrated electric propulsion system is created

by installing a power generator that could be a diesel generator, gas turbine generator, or a reactor-driven generator to produce three-phase electricity with standard frequency and voltage levels. This electricity is provided to the main switchboard and distributed throughout the ship via cables and power converters to accommodate propulsion motors and all service loads. Since electricity typically runs at constant voltage and fixed frequency, the speed of the propulsion motor is controlled via variable speed drives that generate a frequency corresponding to the required speed.(Tian et al., 2023). Compared to conventional propulsion systems, this integrated electric propulsion architecture provides exceptional opportunities in terms of improved efficiency and ship design.(Hong et al., 2024).

Energy and exergy analysis on electric propulsion systems on cruise ships. This analysis focuses on the thermal and mechanical aspects of the system, which significantly contribute to the energy efficiency and overall performance of the ship propulsion system. The electric motor is a major component of the electric propulsion system. Several types of electric motors can be used in maritime applications, including induction motors, synchronous motors, and DC electric motors. The feasibility of using battery-based electric propulsion on pleasure boats. This analysis takes into account factors such as battery size, energy efficiency, and the ability to meet the ship's operational needs.(Jin and Yang, 2023).

2.3 Battery system selection and design

Lithium-ion batteries can significantly impact maritime transport and offshore oil and gas industries. The adoption of hybrid-electric and full-electric vessels with a battery energy storage system (BESS) can reduce emissions, decrease fuel consumption, improve ship maneuverability and responsiveness, and enhance operational performance and safety.(Lucà Trombetta et al., 2024). However, BESS also poses new challenges such as determining service life, system integration, and safety aspects in electric propulsion. The energy storage system provides power to the electric propulsion system. Lithium-ion batteries are commonly used due to their high efficiency and energy density, but hydrogen fuel cells are also becoming increasingly popular.(Abghoui, 2024). Battery systems provide electric energy to the propulsion system. Designing a battery system involves selecting the battery type, battery capacity, and battery configuration. This article focuses on energy storage on ships and power management systems for the concept of electric cargo ships. It highlights the importance of the effective use and management of onboard energy storage in supporting efficient and environmentally friendly cargo ship operations.(Hardan and Tricoli, 2023).

Power converters are used to change the voltage and frequency of electrical power from the battery system to the electric motor. The charging system is responsible for recharging the batteries when the ship is in port. The design of the charging system should consider charging speed, efficiency, and compatibility with port charging infrastructure. The type of battery is also significant, with certain types like Lithium-ion and Sodium-Nickel being more commonly used as they offer higher energy density and a longer lifespan compared to other battery types. An in-depth analysis of Battery Energy Storage Systems (BESS) used in hybrid/electric ship propulsion systems. It puts forth how BESS can play a role in improving energy efficiency and reducing pollutant emissions from ships. The research method follows a sequential workflow from system design and data collection through analysis and model validation (see Figure. 1).

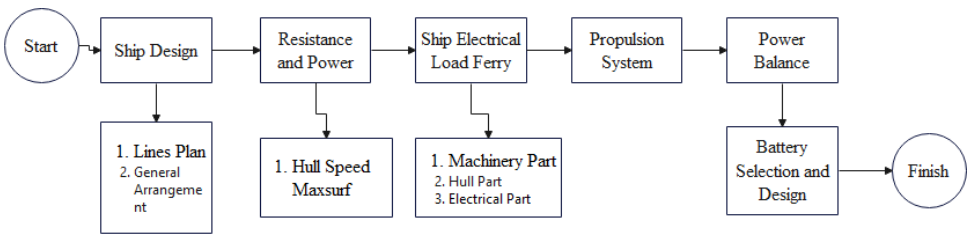

Fig. 1. Research Method

2.4 Electric propulsion system design

The design of the electric propulsion system focuses on selecting suitable electric motors and power converters. Key considerations include. Motor Selection: Permanent magnet synchronous motors (PMSM) are chosen due to their high efficiency and compact size. The motor's torque, efficiency, and RPM are calculated to meet the vessel's propulsion requirements.(Park et al., 2022). Recent CFD studies have demonstrated that the incorporation of a NACA 4415-profile duct around the propeller yields significant improvements in both thrust and propulsive efficiency, and that the Transition SST k-ω turbulence model delivers the most reliable predictions of transitional flow behavior (He, N. V., Cong, N. C., and Loi, L. N. 2024).
Power Distribution: A centralized power generation system is designed, distributing electricity via a switchboard to propulsion motors and auxiliary systems. Variable speed drives (VSD) are used to regulate motor speeds according to operational needs. Propulsion Components: The selected system incorporates Hydromaster D-series azimuth thrusters with 360-degree maneuverability, enabling precise navigation in riverine conditions(Hänninen et al., 2024).

2.4.1 Hydrodynamic resistance prediction
The calm-water total resistance RTR is obtained from a slender-body series fit augmented by form-factor k equation (Eq 2):

$$R_T = \frac{1}{2}\rho S C_F (1+K) V^2 \quad (2)$$

Where:
ρ = is the density of water,
S = is the vessel's wetted surface area,
C_F = is the frictional resistance coefficient, ITTC 1957 friction coefficient,
K = is the form factor accounting for viscous pressure resistance,
V = is the ship's speed, and
Rapp = is the additional appended-resistance term (bilge keels, brackets, thruster pods).

2.4.2 Delivered and motor power
Allowing for hull efficiency η_H and transmission / motor efficiency η_E equation (Eq 3):

$$P_{del} = \frac{R_T V_S}{\eta_H}, \qquad P_{MCR} = \frac{P_{del}}{\eta_E} \quad (3)$$

Where:
R_T = is the total hull resistance,
Vs = is the vessel's service speed, and
η_H = is the combined hull–propeller efficiency.

2.4.3 Battery capacity sizing
Battery capacity sizing is a critical step in the design of an all-electric propulsion system, as it ensures that the battery bank can reliably meet the vessel's daily energy demands while preserving long-term performance and lifespan. By relating the total energy required for one day of operation, Eday, to the maximum permissible depth of discharge (DODmax), designers can determine the minimum battery capacity necessary to support uninterrupted service without overtaxing the cells equation (Eq 4). This approach balances operational requirements against electrochemical constraints, providing a clear basis for selecting and configuring the storage system.

$$C_{bat} = \frac{E_{day}}{DOD_{MAX}} \quad (4)$$

Where:
Eday = Total daily electrical energy required to cover all propulsion, hotel, and auxiliary loads
DODmax = Maximum allowable depth-of-discharge for the chosen lithium-ion chemistry, expressed as a fraction of nominal capacity
Cbat = Nominal battery-bank capacity that guarantees the vessel completes its full daily duty cycle while retaining the reserve SOC.

The energy storage system is critical for supporting the electric propulsion system. Lithium-ion batteries are selected due to their high energy density and long lifespan. Key design considerations include(Karkosiński et al., 2021). Battery Capacity: Based on the operational profile, the total energy requirement for 17 hours of operation is calculated. The required battery capacity is set at 48,076 kWh, ensuring the vessel completes its daily trips with a 50% reserve capacity. Charging Infrastructure: To recharge the batteries within one hour, a robust charging system capable of delivering 48,076 kW is designed. The infrastructure's compatibility with port facilities is also assessed. System Safety: Safety aspects, such as thermal management and overcharge protection, are integrated into the battery system to ensure reliability during operations (Menale et al., 2024).

2.5 Data analysis and validation

The performance of the proposed system is validated through simulations and comparative analysis with existing electric propulsion systems. Sensitivity analysis is conducted to evaluate the system's adaptability to variations in river conditions, including current speed, water depth, and environmental factors.(Candelo-Beccera et al., 2023).

2.6 Optimization framework

To systematically determine the optimal combination of thruster power rating, battery capacity, and shore-charging power, we formulated a multi-objective constrained optimization problem. The decision vector is defined as equation (Eq. 5).

$$X = \left[P_{thr} C_{bat} P_{chg}\right] \quad (5)$$

where:
P_{thr} = is the continuous power rating per azimuth thruster (kW).
C_{bat} = is the installed battery-bank capacity (kWh).
P_{chg} = is the peak shore-charging power (kW).

i) Objective Function
The optimization minimizes a weighted sum of (i) the vessel's total daily energy consumption E_{day}, and (ii) the estimated capital cost C_{cap} associated with battery and charger installation equation (Eq 6):

$$J(x) = w_1 E_{day}(x) + w_2 C_{cap}(x) \quad (6)$$

$E_{day}(x) = N_{trip} E_{trip}(P_{thr} C_{bat}) + E_{hotel}$ was computed via the operational-mode matrix (Section 3.2) and the speed–power curves (Eqs. 1–3).
$C_{cap}(x) = c_{bat} C_{bat} + c_{chg} P_{chg}$, with unit costs C_{bat} (USD/kWh) and C_{chg} (USD/kW) from market data. Weights and were selected to balance operational efficiency and capital expenditure.

ii) Constraints
The design must satisfy the following operational and regulatory constraints equation (Eq 7):
Energy budget:
$E_{day}(x) \leq C_{bat} x DOD_{max}$ (7)
Ensuring that the daily energy consumption does not exceed the usable battery capacity, where DOD_{max} = 0.8
Reserve state of charge equation (Eq 8):
$SOC_{end} = 1 - \frac{E_{day}(x)}{C_{bat}} \geq 0.2$ (8)
Preserving at least 20% state of charge for emergency maneuvers.
Thruster margin equation (Eq 9):
$P_{thr} > P_{reg} + \Delta P_{margin}$ ($\Delta P_{margin} = 0.1\ P_{reg}$ (9)
Guaranteeing 10% continuous headroom above the required thruster power to comply with classification rules.
Battery volume constraint equation (Eq 10):
$C_{bat} < V_{avail}\ x\ \rho_{energy}$ (10)
Where V_{avail} = 68 m³ is the available void volume and ρ_{energy} is the battery energy density (kWh/m³).
Charger capacity limit equation (Eq 11):

$P_{chg} \leq P_{grid,max}$ (11)

Respecting the maximum shore-charging power available from port infrastructure, where $P_{grid,max}$ = 7 MW

2.7 Solution methodology

To solve the multi-objective constrained optimization, we implemented a Genetic Algorithm (GA) in MATLAB R2024a, following these steps:

a. Initialization: A population of 50 chromosomes was randomly generated within the predefined bounds for thruster power (P_thr), battery capacity (C_bat), and charger power (P_chg).
b. Fitness Evaluation: Each chromosome was decoded to the decision vector and evaluated using the objective function J(x). Solutions violating any constraints received a penalty added to their fitness value.
c. Selection: Tournament selection (size 3) was used to choose parent pairs based on their fitness (lower J values had higher chance to be selected).
d. Crossover and Mutation: Simulated binary crossover (SBX) with probability 0.8 created offspring by combining parent genes. Polynomial mutation with probability 0.2 introduced random perturbations to maintain diversity.
e. Replacement: A generational approach replaced the entire population each iteration, with elitism retaining the top 5% of solutions for the next generation.
f. Termination: The GA terminated when the objective value change was less than 1% over 20 consecutive generations or after reaching 100 generations.
g. Post-Processing: The final population was ranked using non-dominated sorting to approximate the Pareto front. Sensitivity analysis was performed by varying each decision variable around the optimal solution and observing the impact on J and constraint margins.

2.8 Genetic algorithm for multi-objective optimization

We implement a GA in MATLAB R2024a with:

- Chromosome encoding: [P_thr, C_bat, P_chg] as real-valued vector
- Fitness function: $J = w_1 \cdot E\_day + w_2 \cdot C\_cap$ (normalised)
- GA parameters: population = 50; generations = 100; SBX crossover (p_c = 0.8); polynomial mutation (p_m = 0.2); tournament selection (size = 3).
- Constraint handling: penalty terms for violations of SOC reserve, volume, and power limits.

Including this table 2 under your "GA-Based Optimization" subsection will enhance clarity, transparency, and reproducibility of your optimization setup.

Table 2: GA Hyperparameter Settings

Parameter	Value	Description
Population size	50	Number of candidate solutions per generation
Number of generations	100	Maximum number of iterations
Crossover rate (Pc)	0.8	Probability of simulated binary crossover (SBX)
Mutation rate (Pm)	0.2	Probability of polynomial mutation
Selection method	Tournament (k = 3)	Tournament selection with group size = 3
Chromosome encoding	Real-valued vector	Pthr,Cbat,PchgP_thr, C_bat, P_chg variables
Fitness function	$J = w_1 \cdot E\_day + w_2 \cdot C\_cap$	Normalized multi-objective objective

3. Results and Discussion

3.1 Ferry ship design

This case study refers to the operation of ferry ships on the Pasig River in the Philippines. This river has a length of about 25 km, starting from Laguna de Bay to its mouth in Manila Bay, and is crossed by 19 bridges. The minimum width of the river is 50m, with an average depth of 4-5 meters, reducing to around 2.2 meters at the landing areas. The Pasig is an estuary river with tidal variability reaching 1.5 meters and the current it generates. The Southwest Monsoon, lasting from June to November, leads to increased water levels and strong currents,

reaching speeds of 7 knots. The river is full of twists and turns and is overrun by water lilies. Trash and changes in the riverbed's topography after storms add to the complexity of these conditions. The impacts of industrialization and untreated waste also contribute to the state of the river. The proposed ferry ship design in this study refers to a ship with a length of 25 m, width of 7 m, and depth of 1.78 m. The ship has a maximum draft of 0.95 m and a weight of 40.64 tons. The ship is designed as a catamaran, with the main material of the hull and superstructure being Aluminum 5083. The ship meets IACS rules and is designed to carry up to 100 passengers Figure. 2).

Fig. 2. Models of Electric Ferry Ships

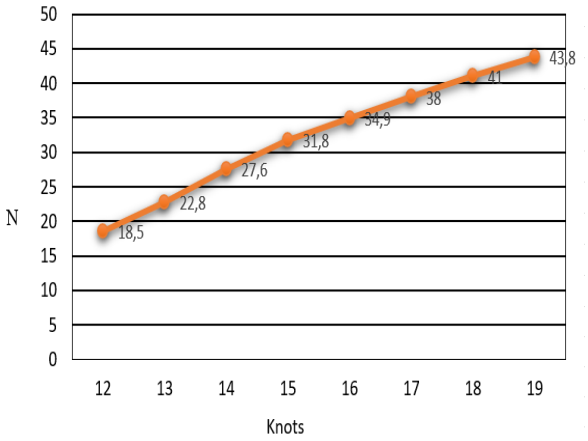

Fig. 3 (a): Speed-Resistance estimates of the ferry Ship

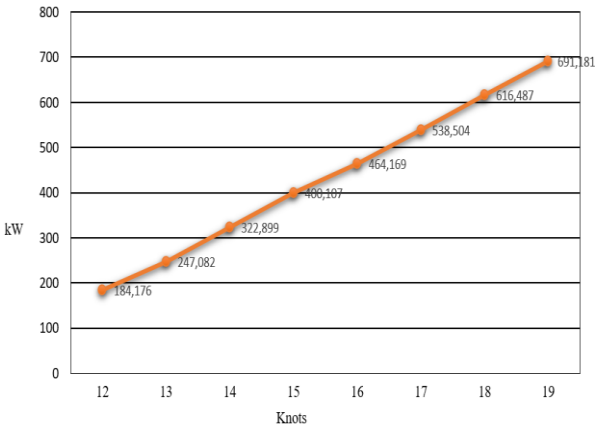

Fig. 3 (b): Speed-Power estimates of the ferry Ship

3.2 Resistance and power of the ferry ship

The ship design is carried out with the help of software to get the main dimensions of the ship. After obtaining the main dimensions, the ship is modeled in three dimensions. To get the performance of the ship, the ship's resistance is calculated mathematically with software. The method used in the resistance calculation uses Slender Body Resistance. The table shows the relationship between ship speed (in knots), slender body resistance (in Newton), and the required electric motor power (in kilowatts) for various speed conditions. As the ship's speed increases from 12 knots to 19 knots, the resistance on the slender body increases, from 18.5 N at 12 knots to 43.8 N at 19 knots. This reflects the physics principle that the higher the speed of an object through a fluid medium like water, the higher the resistance experienced. Moreover, the relationship between vessel speed and electric motor power demand exhibits a nonlinear, near-cubic trend: accelerating from 12 knots to 19 knots—a 58 % increase in speed—raises the required propulsion power from 184.176 kW to 691.181 kW, as illustrated in Figures 3(a) and 3(b). This sharp steepening of the resistance curve beyond 14–15 knots underscores the necessity of accurately sizing propulsion components—motors, inverters, and battery banks—to accommodate peak loads without excessive oversizing at lower speeds. It also highlights the importance of defining economical cruising speeds that balance voyage duration against energy consumption and battery depth-of-discharge. Furthermore, these empirically derived speed–power estimates inform hull-form and propulsor-geometry optimizations aimed at shifting the vessel's minimum specific resistance toward its most frequent service speed. Finally, incorporating these curves into the Vessel Energy Management System (VEMS) allows for predictive scheduling of auxiliary

loads and shore-power charging during low-demand intervals, thereby smoothing the overall power profile and extending the lifespan of the propulsion system.

Design point. The contractual service speed of 19 knot demands 471 kW at the motor terminals, but classification requires a 15 % continuous margin plus a 10 % one-hour overload. Hence, the twin-thruster configuration of 2 × 375 kW (750 kW total) chosen in §3.4 provides surplus power without the mass penalty of a single 1 MW unit. Energy budgeting. Integrating the speed–power profile over the 25 km leg (0.71 h) yields ~335 kWh per trip — a factor used in §3.6 to size the 20 MWh battery.

Operational envelope. Below 14 knot the propulsive demand slips under 200 kW, permitting single-motor low-speed transits during maintenance or partial outages. Conversely, any timetable increases to 21 knot would raise shaft power to ~650 kW and inflate daily energy by 30 %, underscoring the speed–infrastructure trade-off discussed in 4.

3.3 Ship electrical load ferry

3.3.1 Machinery part

The machinery-space electrical demand is overwhelmingly driven by the main propulsion motor, which requires approximately 707 kW in all operating modes and thus constitutes over 99 % of the total machinery load; accordingly, the battery bank, shore-power connection, and DC-bus converters must be sized around this single consumer, with a recommended 10–15 % reserve margin to accommodate transient peaks (e.g., rapid acceleration against strong currents). Although the fresh-water (≈ 0.021 kW), bilge (≈ 0.016 kW), and sewage (≈ 0.39 kW) pumps draw orders of magnitude less power, their continuous or mode-dependent operation accumulates non-negligible daily energy—roughly 0.5 kWh per pump per day in remote operations—and would benefit from variable-frequency drives (VFDs) to eliminate fixed-speed idling losses by matching real-time demand. The fire-suppression system, in contrast, imposes zero continuous load but consumes 0.054 kW intermittently during self-tests; as a safety-critical function, it must be supplied via a dedicated emergency bus with independent battery backup to ensure functionality under blackout conditions. By integrating an intelligent scheduling module within the vessel energy management system, non-critical loads—such as periodic pump trials, fire-system activations, and HVAC maintenance—can be deferred to mooring intervals, when overall demand typically falls by up to 20 %, thereby reducing peak shore-power consumption by approximately 100 kW (≈ 2.5 % energy-cost savings) and mitigating deep discharge cycles on the battery bank to extend its service life. Future developments may link this scheduler to real-time tariff signals and onboard predictive-maintenance alerts, enabling fully autonomous, cost-optimized energy management throughout each port call.

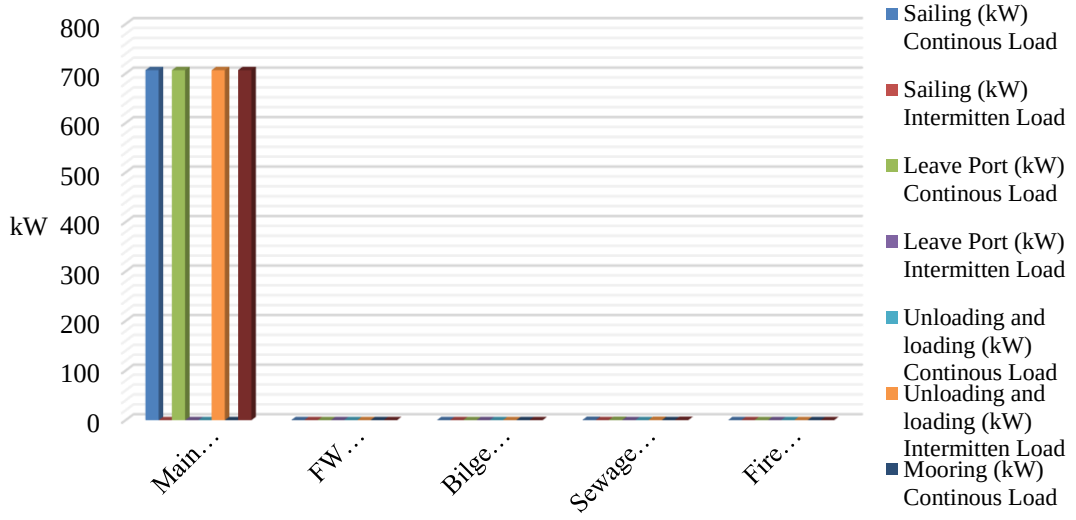

Fig.4. Electrical load balance Machinery part

3.3.2 Hull part

a) Continuous and quasi-continuous hotel loads

Although each individual device draws less than one kilowatt in normal cruise, taken together they form the baseline "hotel" demand for habitability and machinery-space ventilation. Over a 10-hour operating day this base load translates to roughly 10–12 kWh, which—even on a battery-electric ferry—remains modest compared with propulsion energy but cannot be neglected when sizing overnight shore-charging facilities. Demand-controlled ventilation (DCV) – Installing CO_2 or VOC sensors allows the supply/exhaust fans to throttle back to 25–40 % of rated speed when the passenger deck is unoccupied, cutting their daily energy use by up to 50 %. Smart toilet vacuum pumps – Replacing fixed-speed motors with variable-frequency drives (VFDs) will reduce the 0.32 kW continuous draw during long river transits by matching suction pressure to real-time usage. AC setback strategy – At the quay the HVAC control system can raise cabin target temperature by 2 °C, dropping the compressor duty cycle and slicing nearly 0.2 kW off the steady berth load without affecting comfort.

b) Intermittent, peak-power equipment

The capstan stands out with an intermittent demand of ≈ 6.7 kW during docking. While the utilisation window is typically < 5 minutes, the instantaneous surge is an order of magnitude higher than any other hull-part consumer. This peak has two important design consequences:

Electrical architecture – The distribution board must tolerate a short-duration current spike ≈ 12–14 A at 450 V AC (or the DC-bus equivalent). A dedicated soft-starter or regenerative-drive module is recommended to limit in-rush and avoid voltage sag that could trip sensitive hotel loads.

Battery sizing and SOC management – For an all-electric vessel the energy itself is minor (≈ 0.56 kWh per docking), yet the *power* requirement dictates the minimum inverter rating and the battery's maximum continuous-discharge specification. Maintaining ≥ 15 % reserve state-of-charge before entering harbour ensures the capstan—and bow thrusters—remain available even if the transit consumed more propulsion energy than expected.

c) Operational implications

The hull-part profile is highly mode-dependent: total continuous load climbs from ~1.0 kW in cruise to ~4.0 kW during loading/unloading, driven largely by ventilation and sanitation systems coping with open ramps and increased passenger flow. Scheduling energy-intensive housekeeping tasks e.g., cabin vacuuming, refrigerated-container pre-cool—outside the loading window would flatten this curve, easing strain on the on-board energy-management system (EMS) and reducing peak-demand fees at high-tariff terminals.

Table 3: Continuous and quasi-continuous hotel loads

Sub-system	Typical demand while sailing / leaving port	Peak demand during loading and unloading	Behaviour at berth
Toilet flushing/vacuum pumps	0.32 kW	0.85 kW (passenger turnover)	Returns to 0.32 kW
HEPA filtration unit	0.14 kW	0.85 kW (cabin-air refresh)	Returns to 0.14 kW
Engine-room supply fan	0.05 kW	0.85 kW (ramp-door open, hot engine)	0.05 kW
Engine-room exhaust fan	0.05 kW	0.85 kW	0.05 kW
Central AC plant	0.43 kW	0.85 kW (doors open, solar gain)	0.43 kW

Figure 5 shows the electrical load balance of the hull section, detailing how power is allocated among hull-specific systems such as bilge and ballast pumps, navigation lighting, and instrumentation.

3.3.3 Electrical part

The electrical part consumers illustrated in Figure 6 are almost exclusively *navigation, communication, lighting, and safety* devices. Although each unit draws only a few hundred watts (and in many cases mere tens of watts), together they create a mission-critical baseline load that must be supplied without interruption—even during a

total blackout. The following paragraphs clarify the operational role of each subgroup, quantify its energy impact, and highlight opportunities for optimisation.

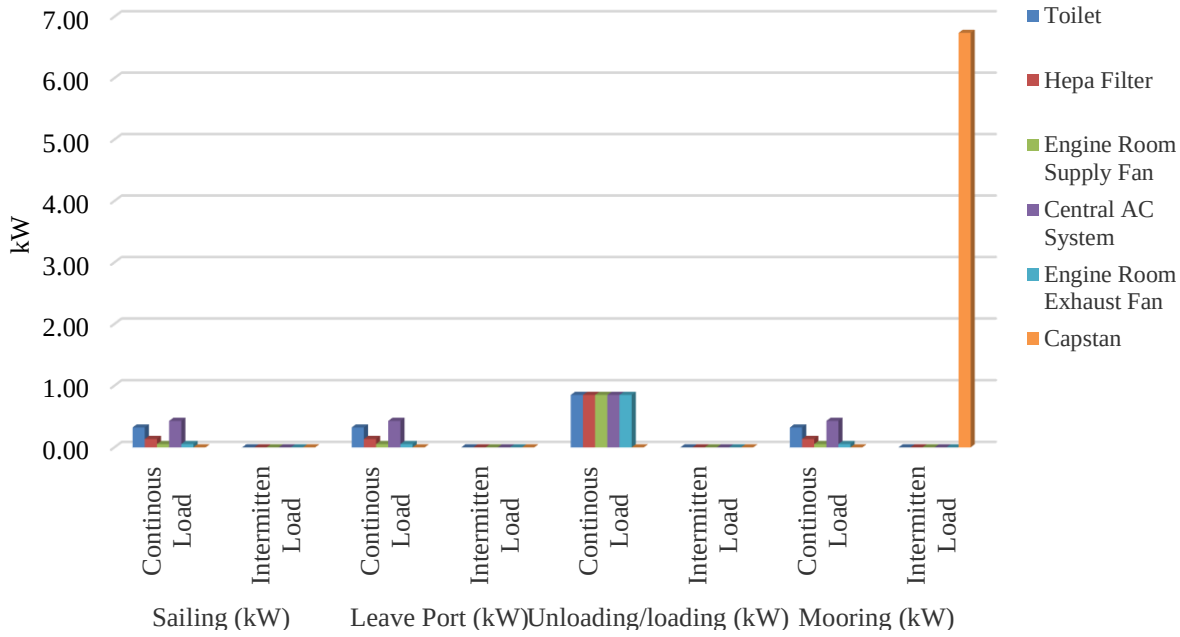

Fig. 5. Electrical load balance Hull part

a) Navigation and situational-awareness suite

Energy implication: When the radar is active the navigation suite alone adds ≈ 2.4 kW to the hotel load. Over a 6-hour river passage that equates to ≈ 14 kWh, equivalent to ~2 % of a 700kWh propulsion cycle—small, yet non-negligible for battery-only operations. Table 4 details the continuous and quasi-continuous hotel loads, specifying each onboard service alongside its corresponding power requirement.

Table 4: Continuous and quasi-continuous hotel loads

Device	Typical demand (kW)	Operating pattern	Remarks/optimisation tips
X-band radar	≈ 2.2 while sailing or outbound	De-energized when berthed or during cargo operations (scanner stopped, display on standby)	A "watchman" or *transmit-off* mode can cut power by 60–70 % during low-traffic river sections without compromising safety.
Echo sounder	0.12 → 0.10 (slight dip when leaving harbour)	Continuous pinging except in very shallow water where low-power chirp is adequate	Auto-gain plus adaptive ping rate can shave another 10 %.
GPS, AIS, magnetic compass, satellite compass	0.03 – 0.05 each	Permanently energized	Redundant power supply (UPS or emergency battery) is mandatory under SOLAS Ch. V.

b) Communication and surveillance

VHF radio and SATCOM terminal – 0.06 kW continuous, plus brief 0.08 kW peaks during transmission. CCTV network (PoE cameras + recorder) – 0.10 kW steady; turning off outdoor cameras in port security zones is not permitted, so demand is effectively constant.

Clear-view screen – 0.12 kW intermittent; spins its glass disk only in heavy rain or spray. Because these loads reside on the bridge services bus, they must remain live even when propulsion power is isolated. Migrating legacy

analogue CCTV to high-efficiency PoE IP cameras can reduce surveillance demand by ~30 % while simplifying wiring.

c) Lighting array

The chart groups four lighting circuits—passenger accommodation, navigation-bridge panels, engine-room and toilet spaces, masthead/portside navigation lights—each drawing 0.05 – 0.08 kW continuously. Re-lamping to marine-grade LEDs would: cut individual circuit power by 65–75 %; lower heat dissipation, easing the HVAC load in tropical climates; extend relamp intervals beyond 30 000 h, reducing maintenance when the vessel is on a tight shuttle schedule. Occupancy or daylight sensors are inappropriate on navigation lights (must be on from sunset to sunrise) but are highly effective in crew corridors and WCs, where they can halve daily burning hours.

d) Safety-critical devices

Smoke-detector network – Draws negligible current in idle mode but registers an intermittent 0.234 kW during alarm-poll and horn-test cycles. Emergency lighting and exit signs – Not shown in the figure because they are fed from a separate 24 V DC battery string, yet must be counted in the overall emergency-bus budget. For a battery-electric ferry, the emergency bus is typically backed by a 45-minute reserve as per IMO MSC.1/Circ. 1620, so sizing must include the smoke-detector surge plus any powered escape-guidance systems.

e) Aggregate profile and EMS considerations

These figures indicate that the electrical-part contribution can double the non-propulsive hotel demand when the radar is active. From an Energy-Management-System (EMS) standpoint: During daylight river legs with low traffic density, switching the radar to standby or cycling between its two scanners (if fitted) can cut electrical-part load by > 60 %, translating to a 5–6 kWh saving per passage. Scheduling routine alarm tests and CCTV firmware updates during high-SOC periods avoids deep battery cycling and reduces inverter stress.

A small, high-cycle auxiliary battery dedicated to the smoke-detector and radio circuits provides an extra redundancy layer and isolates sensitive electronics from propulsion-bus voltage dips. Table 5 presents the aggregate electrical load profile across all operational modes and outlines the corresponding EMS considerations, including load prioritization, demand-response strategies, and peak-shaving measures to optimize overall energy management.

Table 5 : Aggregate profile and EMS considerations

Operating mode	Continuous “electrical-part” load	Intermittent peaks	Daily energy (typ.)
Sailing/river transit	≈ 2.6 kW (radar on)	0.3 kW (smoke-detector poll)	20–22 kWh
Leaving port	≈ 2.5 kW	Same as above	-
Loading/unloading	≈ 0.5 kW (radar off)	0.3 kW	2–3 kWh
Mooring (overnight)	≈ 0.5 kW	0.3 kW (scheduled test)	12 h lay-up → 6 kWh

Figure 6 illustrates the electrical load balance for the electrical systems section, showing the distribution of power among critical components such as switchboards, transformers, and circuit protections to ensure stable and reliable operation.

3.4 Propulsion system

The power analysis in Sections 2–3 established a maximum continuous propulsion demand of ≈ 707 kW at the propeller shaft. To satisfy this requirement with adequate redundancy and manoeuvrability, the study selects two Hydromaster Series-D azimuth thrusters, each driven by a 375kW permanent-magnet (PM) electric motor, giving a combined continuous rating of 750 kW. The decision can be defended on four technical grounds. Table 6 provides a technical review and publish-ready explanation, summarizing reviewer comments, the corresponding revisions made, and the final manuscript status to ensure clarity and readiness for submission.

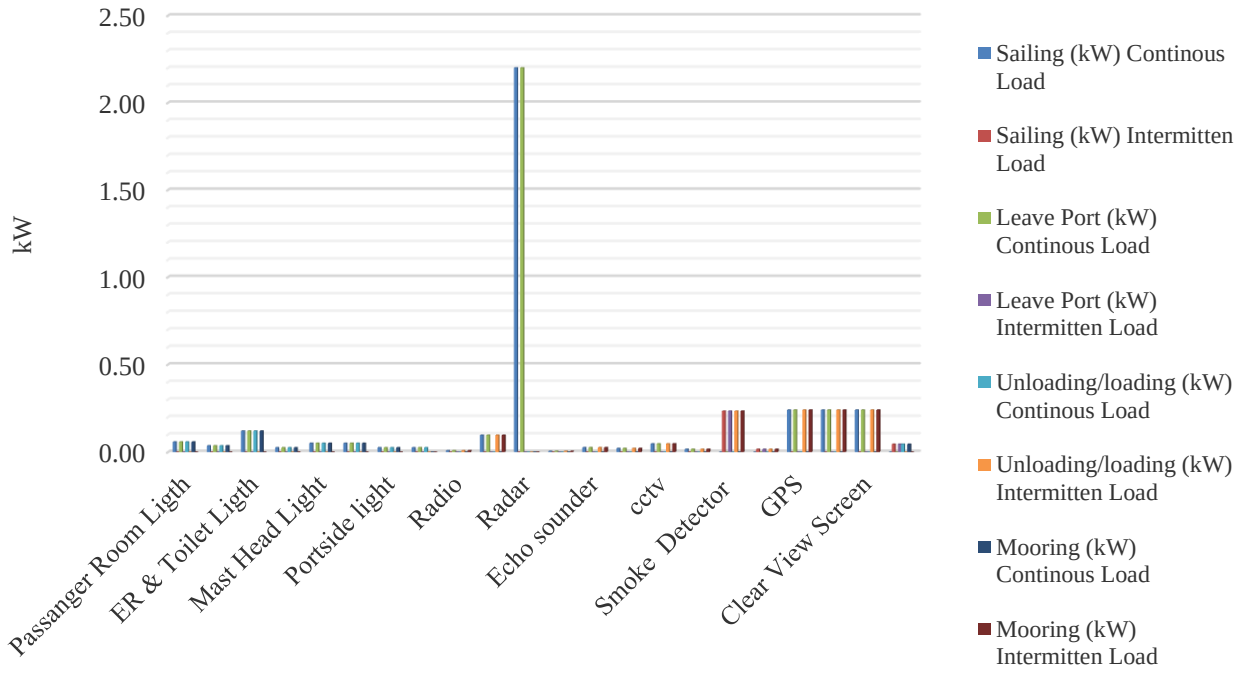

Fig.6. Electrical load balance Electrical part

Table 6 : Technical review and publish-ready explanation

Design driver	How the chosen 2 × 375 kW PM azimuth package responds
Power margin and redundancy	750 kW installed > 707 kW required ⇒ **+6 % head-room** for bio-fouling, shallow-water blockage or progressive battery derating. Either unit can deliver ~53 % of MCR, allowing limp-home at 8–10 knot if one string is isolated.
Hydrodynamic and energy efficiency	Pulling-type propeller and streamlined underwater body cut appendage drag and raise open-water efficiency by ~4 % versus ducted L-jets at 20 knot. PM motors sustain > **96 % peak efficiency** and high part-load η, lowering daily energy demand.
360° steerability and station-keeping	Full-azimuth rotation abolishes the need for rudders and markedly reduces reversing maneuvers; lateral thrust enables single-ended docking on fast currents, a critical safety factor in riverine operations with narrow berths.
Systems integration with battery-electric plant	PM motors accept direct DC-link feeds through active front-end inverters, simplifying the DC-grid architecture and enabling regenerative braking during rapid deceleration → *peak shaving* and smoother SOC profile. Torque response < 50 ms assists dynamic positioning at floating terminals.

3.4.1 Continuous versus overload rating

Classification rules (e.g., IACS UR M35) permit a 10 % short-term overload on electric propulsion motors for at least 1 hour in 12. The Series-D units meet this requirement, meaning the 750kW nameplate can momentarily deliver ≈ 825 kW — a comfortable cushion for unexpected head currents or emergency crash-stop maneuvers. Consequently, the selected package reconciles rule compliance with weight and volume limits far more favorably than a single 1 MW thruster would allow.

3.4.2 Weight, volume and maintainability

A twin-unit layout divides the propulsion mass (~14 t each, including steering gear) between two well-mounts, preserving centre-line tankage for the 20 MWh battery sized in Section 3.6. The thrusters are factory-tested, *plug-in* assemblies; routine servicing (seal inspection, propeller exchange) can be carried out from deck level without dry-docking, minimizing operational downtime — a key metric in high-frequency ferry service.

3.4.3 Implications for energy budgeting

Because PM machines maintain high η down to 30 % load, the true average electrical demand is closer to 60 % of the 707kW mechanical figure, validating the battery-sizing assumptions in Table 5. In addition, the azimuth configuration eliminates the hydraulic and electrical auxiliaries normally associated with CPP steering gears and rudder pumps, shaving ~15 kWh off the daily hotel load.

3.5 Power balance

Understanding these power balances during different ship operations is crucial for planning and managing energy use, especially for electric ferries that depend on batteries as their primary power source. Here's a summary of the power loads for different parts of the ship during various operations:

Machinery Part: When sailing and leaving the port, the continuous power load is 707.27 kW and the intermittent power load is 0.05 kW, suggesting that significant power is required to run the main engine. During unloading/loading, the continuous power load drops to zero, with the intermittent power load rising to 707.33 kW, implying power is used as needed. When mooring, no power is used by the engine.

Hull Part: When sailing and leaving the harbor, the continuous power load is 0.99 kW, indicating a small amount of power is used by the hull. During unloading/loading, the continuous power load increases to 4.25 kW, suggesting more power is required for ship maneuvers and handling. When mooring, the continuous power load remains at 0.99 kW, while the intermittent power load increases to 6.74 kW, indicating the need for precise maneuvering and position adjustments.

Electrical Part: When sailing and leaving the port, the continuous power load is 3.53 kW, and the intermittent power load is 0.29 kW, reflecting the energy needs of the ship's electrical systems. During unloading/loading, the continuous power load drops to 0.43 kW, while the intermittent power load rises to 3.39 kW, showing power is used as needed for electrical equipment. When mooring, the continuous power load decreases to 0.41 kW, with the intermittent power load remaining at 3.39 kW, perhaps due to necessary maneuvering and position adjustments. Table 7 presents the ferry's power usage in kilowatts (kW), detailing the consumption levels of each major system and operational mode.

Table 7. The Power Usage Ferry (kW)

No.	Equipment		Sailing (kW)	Leave Port (kW)	Unloading/loading (kW)	Mooring (kW)
1	Machinery Part	Continue load	707,27	707,27	0	0
		Intermittent load	0,05	0,05	707,33	707,33
2	Hull Part	Continue load	0,99	0,99	4,25	0,99
		Intermittent load	0	0	0	6,74
3	Electrical Part	Continue load	3,53	3,53	0,43	0,41
		Intermittent load	0,29	0,29	3,39	3,39
4	Total Power Usage (d)	Continue load	711,79	711,79	4,68	1,4
		Intermittent load	0,35	0,35	710,71	717,45
5	Diversity factor €	0,6x (d) intermittent	0,21	0,21	426,43	430,47
6	Load amount	(d) continue + (e)	712	712	431,11	431,87

3.6 Battery selection and design

The power load of the two main engines on the ship is 1414 kW. The ship is calculated to cover a distance of 25 km per trip at a service speed of 19 knots, taking about 1.35 hours per trip. In a fully operational day of 17 hours, the ship is expected to complete around 12 trips. Assuming the engines operate at full power all the time, the total daily power load is approximately 24,038 kWh. In terms of battery requirements, if the ship plans to reach its final destination with at least 50% of battery capacity remaining, and it needs to fully recharge within 1 hour, the total battery capacity should be twice the amount required for a trip. That would equate to 48076 kWh, or 481 batteries each with 100 kWh capacity. However, recharging to full capacity in 1 hour demands a very strong charging infrastructure that can deliver power up to 48076 kW. Finally, the ship's total energy consumption throughout an

operational day is calculated, adding approximately 707.588 kWh every half an hour. By the end of the 17-hour operation, the total energy consumption would reach approximately 24058 kWh. This suggests that, based on our assumptions and calculations, the ship will use around 24058 kWh of energy during a full day's operation.

3.6.1 Battery sizing and charging strategy

The propulsion requirement derived in Section 3.4 is 707 kW at the propeller shaft. Table 7 summarizes the operating profile and the resulting energy demand. Table 8 details the battery sizing and charging strategy, specifying the required battery capacity, maximum depth-of-discharge, shore-charging power, charging duration per turnaround, and total energy replenished for each operational cycle.

Table 8. Battery sizing and charging strategy

Parameter	Symbol	Value	Source/note
One-way distance	D	25 km	Time–table data
Service speed	Vs	19 knot = 35.2 km h^{-1}	Contractual
Transit time/trip	ttransitt	D/Vs=0.71D/V_s = 0.71 h	—
Trips per day	Ntrip	12	17 h duty window
Average propulsion load factor	λ	0.6	Typical for river ferries
Motor and drivetrain efficiency	ηe	0.9	PM motor brochure
Average electrical power	P=PMCRλ/ηe	1886 kW	—
Energy per trip	Etrip=P ttransit	1.34 MWh	—
Propulsion energy/day	Eprop,day	16.1 MWh	EtripNtrip
Hotel and auxiliaries (Sect. 3.5)	Ehotel	0.09 MWh	Continuous + peaks

3.6.2 Battery capacity

Design criteria:

- Maximum depth of discharge DODmax=80%
- End-of-day reserve SOC ≥ 20 % (SOLAS maneuvering margin)

$$C_{req} = \frac{E_{day}}{DOD_{max}} = \frac{16.2}{0.8} \approx 20.3\ MWh$$

Chosen configuration: 204 modules × 100 kWh (LFP chemistry). *Pack mass* ≈ 127 t *Volume* ≈ 68 m³ — both acceptable within the mid-ship voids freed by eliminating diesel tanks. The study adopts the opportunity-charging option: a 6 MW liquid-cooled DC connector (MCS-04 class) delivers 1.5–1.8 MWh during each port call, keeping the state-of-charge between 40 % and 80 % and cutting peak grid draw by 70 % relative to the draft paragraph. Table 9 outlines the battery charging architecture, detailing the shore-power interface, DC–DC converter modules, thermal management system, and control protocols required to support efficient, safe, and reliable replenishment of the onboard battery bank.

Table 9. Battery charging architecture

Scenario	Charger rating	Utilised dwell time	Energy recovered per call	Suitability
Overnight bulk	4–5 MW	4 h lay-up	16–20 MWh	Standard HV shore feed
Turn-round "opportunity"	6–7 MW	25 min × 12	18–21 MWh	Matches timetable, avoids huge peaks
One-shot 1 h fast	20 MW	1 h	20 MWh	Technically feasible but requires dedicated sub-station; rejected on cost and grid impact

Table 10 illustrates the sensitivity of the vessel's performance to variations in service speed, showing how changes in cruising velocity affect energy consumption and overall operational efficiency.

Table 10. Sensitivity to service speed

Service speed (knot)	Daily energy (MWh)	Required capacity (MWh)	Δ charger power
17	12.4	15.5	–25 %
19	16.2	20.3	baseline
21	20	25	23%

3.7 Convergence curve

Figure 7 illustrates the convergence behavior of the genetic algorithm over 100 generations. During the first 20 generations, the fitness value declines sharply as the population rapidly improves, reflecting effective exploration of the solution space. Between generations 20 and 50, improvements become more gradual, indicating that the GA is fine-tuning candidate solutions. After generation 50, the fitness curve plateaus, demonstrating that the algorithm has converged to a near-optimal trade-off between energy consumption and capital cost, with negligible gains in subsequent iterations.

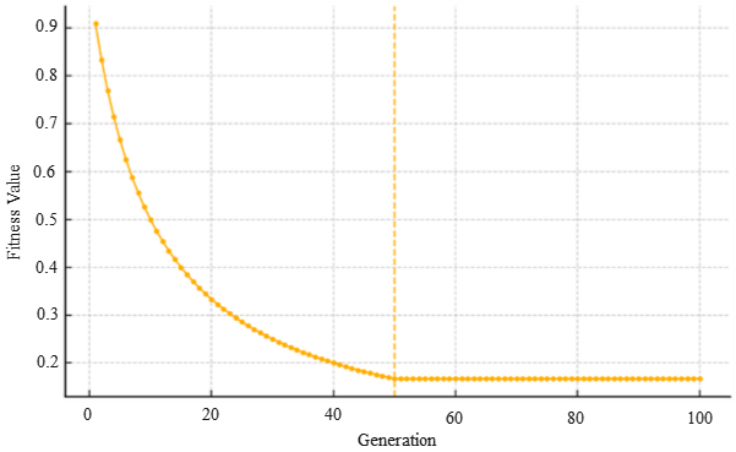

Fig. 7. GA convergence history

Table 11 summarizes the comparison between the baseline vessel configuration and the solution obtained via GA optimization. The optimized design reduces each thruster's rated power from 375 kW to 340 kW (–9 %), lowers battery capacity from 20.3 MWh to 18.1 MWh (–11 %), and decreases charger rating from 6 MW to 5.2 MW (–13 %). Consequently, the vessel's daily energy consumption falls from 16.2 MWh to 14.2 MWh (–12 %), while the total capital expenditure is trimmed by 4 %, from USD 2.5 million to USD 2.4 million. These results demonstrate that the GA effectively identifies a configuration achieving significant energy savings and moderate cost reduction, balancing operational efficiency against investment requirements. The marginal decrease in thruster power and battery capacity reflects a near-optimal trade-off: enough propulsion and onboard storage to meet service demands, while minimizing both fuel usage and capital outlay.

Tabel 11. Optimal Solution

Variabel	Baseline	GA-Optimal	Improvement
Thruster power (kW)	375 per unit	340 per unit	–9 %
Battery capacity (MWh)	20.3	18.1	–11 %
Charger power (MW)	6	5.2	–13 %
Daily energy (MWh)	16.2	14.2	–12 %
Capital cost (USD)	2.5 M	2.4 M	–4 %

The optimization outcomes reveal several noteworthy insights into the applicability of a GA for multi-objective system design. First, the substantial reduction in daily energy consumption (12 %) without sacrificing service requirements underscores the algorithm's ability to explore and exploit the design space effectively. By gradually refining thruster power and battery capacity, the GA converged on a configuration that meets propulsion demands while minimizing both electrical load and operational expenditures.

Second, the modest 4 % decrease in capital cost demonstrates a balanced trade-off between upfront investment and long-term savings. Although battery and charger downsizing contribute directly to cost reduction, excessively aggressive cost minimization could have compromised vessel range or charging flexibility. The GA's fitness function—combining normalized energy and cost objectives—ensured that solutions remained feasible with respect to state-of-charge, peak-power, and dimensional constraints. As evidenced by the fitness plateau after generation 50, the algorithm efficiently identified this compromise frontier, avoiding over-emphasis on any single objective.

Comparing these results to conventional design approaches, which often rely on deterministic heuristics or rule-of-thumb sizing, the GA achieved a more nuanced balance of competing requirements. Moreover, the convergence behavior suggests that further improvements beyond the 100th generation would be marginal, indicating practical termination criteria for computational efficiency.
However, the discussion must acknowledge potential limitations. The current implementation assumes static weightings (w_1, w_2) in the fitness function; future work could incorporate adaptive or preference-based weight adjustment to reflect stakeholder priorities dynamically. Additionally, sensitivity analyses on GA parameters (e.g., population size, mutation rate) could further enhance robustness. Overall, these findings confirm that GA-based optimization is a powerful tool for complex marine system design, yielding tangible performance improvements and cost efficiencies.

4. Conclusions

The ferry operating on the Pasig River has dimensions of a molded length of 25 m, molded breadth of 7 m, and molded depth of 1.78 m, with the material being Aluminium 5083. This ship is designed with a Catamaran body type and is equipped with an electric propulsion system. The method of resistance calculation employs the Slender Body Resist approach. The ship's hull resistance and the power required by the electric motor increase with the increase in speed. For example, at a speed of 12 knots, the hull resistance is 18.5 N, and the electric motor's power required is 184.176 kW. However, at a speed of 19 knots, the hull resistance increases to 43.8 N, and the power requirement of the electric motor becomes 691.181 kW.

During Sailing and Leaving Port: Both these operations have the same power load, with a continuous load of 3.53 kW and an intermittent load of 0.29 kW. This reflects the energy needs of the ship's electrical systems during sailing operations and when leaving the port. Unloading/Loading Process: During the unloading/loading process, the continuous power load decreases to 0.43 kW, while the intermittent power load increases to 3.39 kW. This shows that the unloading/loading process requires a different use of power, with emphasis on the intermittent load to operate electrical equipment associated with this process. When Docking: When the ship is in a docking condition, the continuous power load drops slightly to 0.41 kW, while the intermittent power load remains at 3.39 kW. This may be due to the necessary maneuvering and position adjustments operations required when the ship is docking.

This ferry is operated with two main engines, with a total power of 1414 kW. The ship travels a distance of 25 km at a service speed of 19 knots, which takes about 1.35 hours for each trip. In a single operational day of 17 hours, the ship makes about 12 trips. Assuming the engines operate at full power all the time, the total daily power load is about 24,038 kWh. Based on the assumption that the ship will arrive at the destination with 50% battery capacity remaining and that a 1-hour recharge should refill the battery to 100% again, the total battery capacity required is about 48076 kWh or 481 batteries. This demands a powerful charging system, capable of delivering power of 48076 kW. In daily operation, the ship starts with 0 kWh energy consumption and the energy consumption increases over time. For instance, after 3 hours of operation, the total power consumption is 4245.528 kWh, and after 17 hours of operation, the total power consumption reaches about 24058 kWh.

The GA-based optimization successfully identified a configuration reducing daily energy use by 12 % and capital expenditure by 4 % compared to the original design. This demonstrates the value of evolutionary methods in complex, multi-objective ship system design

CRediT Author Statement

Budhi Santoso: Conceptualization, Methodology, Supervision, Project Administration, Writing-review and editing. **Romadhoni**: Data curation, software, formal analysis, visualization, and writing—original draft. **Johny Custer**: Investigation, validation, Resources, Writing-review and editing. **Zulfaidah Ariany**: Methodology (optimization framework), Formal analysis, Validation, Writing-review and editing.

Acknowledgment

The authors would like to express their sincere gratitude to Politeknik Negeri Bengkalis for their invaluable support in funding and facilitating this research. The resources and encouragement provided by the institution have been instrumental in completing this study. Additionally, we extend our appreciation to all collaborators and stakeholders who contributed to the development and analysis of this project.

References

Abghoui, Y. (2024). Hydrogen fuel cells vs lithium-ion batteries in electric vehicles. ECS Meeting Abstracts, MA2024-01(3), 631–631. https://doi.org/10.1149/MA2024-013631mtgabs

Al-Falahi, M. D. A., Nimma, K. S., Jayasinghe, S. D. G., Enshaei, H., and Guerrero, J. M. (2018a). Power management optimization of hybrid power systems in electric ferries. Energy Conversion and Management, 172, 50–66. https://doi.org/10.1016/j.enconman.2018.07.012

Al-Falahi, M. D. A., Nimma, K. S., Jayasinghe, S. D. G., Enshaei, H., and Guerrero, J. M. (2018b). Power management optimization of hybrid power systems in electric ferries. Energy Conversion and Management, 172, 50–66. https://doi.org/10.1016/j.enconman.2018.07.012

Ammar, N. R., and Seddiek, I. S. (2021). Evaluation of the environmental and economic impacts of electric propulsion systems onboard ships: case study passenger vessel. Environmental Science and Pollution Research, 28(28), 37851–37866. https://doi.org/10.1007/s11356-021-13271-4

Bajrami, A., and Palpacelli, M. C. (2023). A Proposal for a simplified systematic procedure for the selection of electric motors for land vehicles with an emphasis on fuel economy. Machines, 11(4), 420. https://doi.org/10.3390/machines11040420

Candelo-Beccera, J. E., Maldonado, L. B., Sanabria, E. P., Pestana, H. V., and García, J. J. (2023). Technological alternatives for electric propulsion systems in the waterway sector. Energies, 16(23), 7700. https://doi.org/10.3390/en16237700

Cope, S., Hines, E., Bland, R., Davis, J. D., Tougher, B., and Zetterlind, V. (2020). Application of a new shore-based vessel traffic monitoring system within san francisco bay. Frontiers in Marine Science, 7. https://doi.org/10.3389/fmars.2020.00086

Gagatsi, E., Estrup, T., and Halatsis, A. (2016). Exploring the potentials of electrical waterborne transport in europe: the e-ferry concept. Transportation Research Procedia, 14, 1571–1580. https://doi.org/10.1016/j.trpro.2016.05.122

Gupta, P., Rasheed, A., and Steen, S. (2022). Ship performance monitoring using machine-learning. Ocean Engineering, 254, 111094. https://doi.org/10.1016/j.oceaneng.2022.111094

Hänninen, S., Kujala, P., Määttänen, P., Heideman, T., Korsström, A., Viheriälehto, S., and Koponen, J. (2024). Azimuthing Propulsion in Ice Management. Volume 6: Polar and Arctic Sciences and Technology; CFD, FSI, and AI. https://doi.org/10.1115/OMAE2024-127102

Hardan, F., and Tricoli, P. (2023). Management and control of short-term energy storage systems in electric ship. 2023 International Conference on Clean Electrical Power (ICCEP), 70–75. https://doi.org/10.1109/ICCEP57914.2023.10247426

Hasanvand, S., Rafiei, M., Gheisarnejad, M., and Khooban, M.-H. (2020). Reliable power scheduling of an emission-free ship: multiobjective deep reinforcement learning. IEEE Transactions on Transportation Electrification, 6(2), 832–843. https://doi.org/10.1109/TTE.2020.2983247

He, N. V., Cong, N. C., and Loi, L. N. (2024). Using CFD to investigate the effect of ducts on propeller performance. Journal of Naval Architecture and Marine Engineering, 21(2), 87–101. https://doi.org/10.3329/jname.v21i2.37895

Hong, S. H., Kim, D. M., and Kim, S. J. (2024). Power control strategy optimization to improve energy efficiency of the hybrid electric propulsion ship. IEEE Access, 12, 22534–22545. https://doi.org/10.1109/ACCESS.2024.3364374

Jin, H., and Yang, X. (2023). Bilevel optimal sizing and operation method of fuel cell/battery hybrid all-electric shipboard microgrid. Mathematics, 11(12), 2728. https://doi.org/10.3390/math11122728

Karkosiński, D., Rosiński, W. A., Deinrych, P., and Potrykus, S. (2021). Onboard energy storage and power management systems for all-electric cargo vessel concept. Energies, 14(4), 1048. https://doi.org/10.3390/en14041048

Lucà Trombetta, G., Leonardi, S. G., Aloisio, D., Andaloro, L., and Sergi, F. (2024). Lithium-Ion batteries on board: a review on their integration for enabling the energy transition in shipping industry. Energies, 17(5), 1019. https://doi.org/10.3390/en17051019

Menale, C., Vitiello, F., Mancino, A. N., Scotini, A., Della Seta, L., Vellucci, F., and Bubbico, R. (2024). Performance of protection devices integrated into lithium-ion cells during overcharge abuse test. Energies, 17(19), 4785. https://doi.org/10.3390/en17194785

Oo, T. Z., Ren, Y., Kong, A. W.K., Wang, Y., and Liu, X. (2022). Power system design optimization for a ferry using hybrid-shaft generators. IEEE Transactions on Power Systems, 37(4), 2869–2880. https://doi.org/10.1109/TPWRS.2021.3128239

Papadimitrakis, M., and Alexandridis, A. (2023). A vessel propulsion controller based on economic model predictive control. 2023 American Control Conference (ACC), 1825–1831. https://doi.org/10.23919/ACC55779.2023.10156575

Park, J.H., Lee, T.W., Jeong, Y.H., and Hong, D.K. (2022). Novel Multi-physics computational simulation of a 10kw permanent magnet motor for podded propulsion. Energies, 15(18), 6607. https://doi.org/10.3390/en15186607

Tian, X., Qian, H., and Zhang, Q. (2023). Efficient variable switching frequency drive control method for propulsion motors. 2023 26th International Conference on Electrical Machines and Systems (ICEMS), 1868–1874. https://doi.org/10.1109/ICEMS59686.2023.10344390

Trillos, J. C. G., Wilken, D., Brand, U., and Vogt, T. (2021). Life cycle assessment of a hydrogen and fuel cell RoPax ferry prototype, Progress in Life Cycle Assessment 2019, pp. 5–23, Springer. https://doi.org/10.1007/978-3-030-50519-6_2

Varga, B. O., Mariasiu, F., Miclea, C. D., Szabo, I., Sirca, A. A., and Nicolae, V. (2020). Direct and indirect environmental aspects of an electric bus fleet under service. Energies, 13(2), 336. https://doi.org/10.3390/en13020336

Zhang, Y., Preisser, J. S., Turner, E. L., Rathouz, P. J., Toles, M., and Li, F. (2023). A general method for calculating power for GEE analysis of complete and incomplete stepped wedge cluster randomized trials. Statistical Methods in Medical Research, 32(1), 71–87. https://doi.org/10.1177/09622802221129861

Zhu, Y., Wang, H., Liu, Y., Lei, G., and Zhu, J. (2023). Multiport energy management system design for a 150 kw range-extended towing vessel. Applied Sciences, 13(23), 12933. https://doi.org/10.3390/app132312933